JOURNAL OF Applied Polymer SCIENCE

Elongational Rheology of Biodegradable Poly(lactic acid)/Poly[(butylene succinate)-*co*-adipate] Binary Blends and Poly(lactic acid)/Poly[(butylene succinate)-*co*-adipate]/Clay Ternary Nanocomposites

Hassan Eslami, Musa R. Kamal
Department of Chemical Engineering, McGill University, Montreal, Quebec H3A 2B2, Canada
Correspondence to: M. R. Kamal (E-mail: musa.kamal@mcgill.ca)

ABSTRACT: A series of blends based on poly(lactic acid) (PLA) and poly[(butylene succinate)-*co*-adipate] (PBSA) as well as their nanocomposites with nanoclay (PLA/PBSA/Clay ternary nanocomposites) were prepared using the twin-screw extruder. The blends were prepared for PBSA contents ranging from 25 to 75 wt % and their corresponding nanocomposites were prepared at a single-clay concentration. The morphology and structure of the blends and the nanocomposites were examined using field emission scanning electron microscopy, transmission electron microscopy, and X-ray diffraction. Rheological properties (dynamic oscillatory shear measurements and elongational viscosities) of the blends, nanocomposites, and pure components were studied in detail. The strain hardening intensity of different blends and nanocomposites was compared with the behavior of the pure components. Strong strain hardening behavior was observed for blends composed of 50 wt % and higher PBSA content. However, the effect of PBSA content on the elongational viscosity was less pronounced in PLA/PBSA/Clay ternary nanocomposites. © 2012 Wiley Periodicals, Inc. J. Appl. Polym. Sci. 000: 000–000, 2012

KEYWORDS: blends; nanocomposites; rheology; morphology; biodegradable

Received 20 September 2011; accepted 9 March 2012; published online
DOI: 10.1002/app.37928

INTRODUCTION

Poly(lactic acid) (PLA), a linear aliphatic polyester, is one of the most promising renewable biodegradable polymers. Properties such as high gloss and clarity, high tensile strength, good heat sealability, and low coefficient of friction make PLA a suitable candidate for a wide variety of packaging applications.[1] However, drawbacks such as brittleness, low-heat distortion temperature, and high gas/liquid permeability (weak barrier properties) limit its end-use applications, particularly for flexible food packaging. Moreover, PLA does not offer the processability needed for many polymer processing operations (e.g., film blowing, stretch blow molding, foaming, fiber spinning, etc.) owing to its low melt strength. On the other hand, there exist some synthetic biodegradable polymers (e.g., poly[(butylene succinate)-*co*-adipate] (PBSA), a commercially available aliphatic copolyester, poly[(butylene adipate)-*co*-(butylenes terephthalate)] (PBAT), a commercially available aliphatic–aromatic copolyester) with high ductility and good processability. Therefore, blending PLA with such synthetic biodegradable polymers could provide one way of achieving adequate ductility and processability without compromising biodegradability. Along these lines, Lee and McCarthy[2] prepared blends of PLA with chemically modified polyhydroxyoctanoate (mPHO) by direct melt mixing. To improve the compatibility of PLA and PHO, they used hexamethylene diisocyanate as a chain extender for PHO. They reported that the elastic modulus of PLA decreased and its elongation at break increased as mPHO content increased. Wang and Mano[3] employed the solvent casting method to prepare PLA/PBSA blends with various compositions. They observed two independent glass transition temperatures and a biphasic melt was observed for all compositions of the blends, indicating immiscibility of the components. They reported that, when PLA was the major phase, varying the content of PBSA had no significant effect on the mechanism or the rate of crystallization of PLA. However, when PLA was the minor phase, the crystallization rate of PBSA decreased with an increase in PLA content. Rheological, morphological, and mechanical properties of a binary blend of PLA and PBSA were also investigated by Lee and Lee.[4] It was found that as PBSA content increased, no significant improvement was observed in mechanical properties of the blends. The authors suggested that the mechanical properties of PLA/PBSA blends may be improved by

functionalization at the dispersed phase surface, by physical blending with the compatibilizer and/or *in situ* compatibilization. Recently, the dynamic rheological behavior and morphology of PLA/PBAT binary blends with a wide range of compositions were investigated by Li et al.[5] They found that when the PBAT content was lower than 20 wt %, fine and uniform droplet morphology was obtained. Cocontinuous phase structure was observed when the PBAT content reached 50 wt %. The blend structure reverted to the droplet morphology when the PBAT content exceeded 70 wt %. The effects of the different morphologies (e.g., droplet, cocontinuous) on the rheological properties of the blends were also discussed.

Recently, a considerable amount of work has been devoted to a new class of polymer composites, so-called nanocomposites, in which particles with at least one dimension in nanometric size are dispersed in the polymer matrix. Polymer/layered silicate (PLS) nanocomposite is a well-known example of these materials.[6] Special attention has been paid to PLS nanocomposites because of their potential to create materials with enhanced thermal and dimensional stability, lower permeability, better surface finishing and surface printability, and enhanced mechanical properties.[6–11] Ternary nanocomposites, based on polymer blends, have also received attention owing to the possible synergetic effects between the nanoparticles and the structure of the blends.[12] A combination of advanced processing techniques and detailed nanostructure characterizations has made it possible to develop high-performance biodegradable polymer nanocomposites. Kumar et al.[13] prepared PLA/PBAT blends and corresponding nanocomposite using glycidyl methacrylate (GMA) as a reactive compatibilizer to improve the interfacial adhesion between PLA and PBAT. Their results revealed that a PLA/PBAT blend with 25 wt % PBAT exhibited maximum impact strength. Moreover, incorporation of GMA and nanoclay in the blend caused an increase in the impact strength. Ko et al.[14,15] investigated the rheology and morphology of PLA/PBAT/multiwalled carbon nanotube (MWCNT) nanocomposites. Their results showed that PLA/PBAT blends were immiscible. Moreover, MWCNT showed better affinity to the PBAT phase than the PLA phase, owing to the chemical structure of PBAT with aromatic molecules. The authors then concluded that viscosity ratio, flexibility of the polymeric chain, and polymer chemical structure had an important influence on locating MWCNT in the PBAT phase. The shear thinning, elastic and viscous behavior of the nanocomposites confirmed that filler–filler and polymer–filler interactions are very important in determining the location of filler within the system. More recently, Wu et al.,[16] studied the selective localization of some nanofillers in PLA/PCL blends. They reported that clay platelets were mainly located in the PLA phase and at the interface. However, carbon nanotubes were selectively located in the PCL phase and at the interface when the viscosity ratio of the blend components was high. By reducing the viscosity ratio, carbon nanotubes changed their location from the PCL phase to the PLA phase. They then concluded that the selective localization of the nanofillers may not be controlled only thermodynamically through the surface properties of the components but may also be controlled kinematically through viscosity ratio of the blend components. Moreover, it was found that the location of nanofillers had a strong influence on the crystallization behavior within ternary nanocomposites.

The effect of organically modified clay on the morphology of immiscible polymer blends was investigated by Hong et al.[17] They reported that when a small amount of clay platelets was added to the blend, clay platelets were mainly located at the phase interface. This resulted in the suppression of the coalescence of the droplets, which in turn led to a reduction of the droplet size. They also found that, with increasing clay concentration, the clay platelets were localized in the component with stronger affinity to the organically modified clay. The clay platelets caused a change in the viscosity ratio of the blend components. This, in turn, influenced the droplet size in the final morphology. They concluded that clay platelets suppressed the coalescence of the droplets at the interface and influenced the breakup of the droplets owing to the change of viscosity ratio of the blend. Bose et al.[18] investigated the possibility of using the phase separation process as a tool to control the dispersion of MWCNTs in polymer blends. They used amine-functionalized MWCNTs in poly[(*R*-methyl styrene)-coacrylonitrile]/poly (methyl methacrylate) (PRMSAN/PMMA) blends. Their results demonstrated that, as a result of phase separation, it was possible to obtain well-dispersed MWCNTs in PRMSAN/PMMA blends. This resulted in more effective percolation.

Although a considerable amount of work has been devoted to biodegradable polymer blends and their nanocomposites, less attention has been paid to the biodegradable polymer nanocomposite based on the blend of PLA and PBSA. Only a few attempts have dealt with PLA/PBSA blends.[4,19,20] To the best of our knowledge, no research has been done regarding the elongational flow properties of PLA/PBSA blends and PLA/PBSA/Clay nanocomposites. Therefore, the objective of this study has been to prepare biodegradable PLA/PBSA binary blends and PLA/PBSA/Clay ternary nanocomposites and to investigate in detail their rheological properties, particularly their elongational flow behavior.

EXPERIMENTAL

Materials

PLA used in this study was supplied by Natureworks, LLC, USA with the designation 4042D. It is recommended for biaxially oriented films for potential application in packaging. PLA is synthesized by ring opening polymerization of lactides or condensation polymerization of lactic acid monomers.[15] The chemical structure of PLA is shown in Scheme 1.

Synthetic biodegradable PBSA (Bionolle 3001 M) was obtained from Showa High Polymer, Japan. According to the supplier, PBSA has mass density of 1230 kg/m^3. PBSA is a random copolyester synthesized by polycondensation of 1,4-butanediol in the presence of succinic and adipic acids. The production cost of PBSA is relatively low. The mechanical properties and the processability of PBSA are comparable to those of polyolefins.[7] It contains highly flexible macromolecules with excellent impact strength. The chemical formula of PBSA is shown in Scheme 2.

Organically modified montmorillonite used in this study was Cloisite 30B (C30B), supplied by Southern Clay Products, USA.

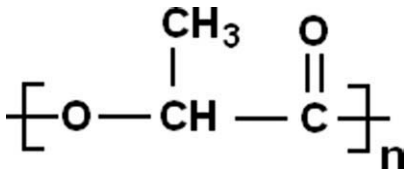

Scheme 1. The chemical structure of PLA.

Cloisite 30B is treated with a methyl, tallow, *bis*(2-hydroxyeethyl) quaternary ammonium chloride surfactant. It has been shown that Cloisite 30B is effective in conjunction with PBSA because of the strong interaction between the "CO" group on the PBSA and the diols on the Cloisite 30B.[7,8,21] All materials (PLA, PBSA, and C30B) were dried under vacuum at 60°C for 72 h prior to processing.

Blending and Nanocomposite Preparation

Extrusion was carried out using a Leistritz 18HP corotating twin-screw extruder ($D = 18$ mm, $L/D = 40$) equipped with eight controllable heating zones. It was followed by a strand die, water bath, and pelletizer. To avoid any possible degradation, the strand was initially cooled by high-pressure air before passing through the water bath. Blends of PLA and PBSA with different compositions were prepared (PLA/PBSA: 75/25, PLA/PBSA: 50/50, and PLA/PBSA: 25/75). First, granules of PLA and PBSA were hand mixed in a plastic container. The hand-mixed samples were then processed using the twin-screw extruder. For the preparation of the nanocomposite, a masterbatch based on PLA was prepared by feeding PLA pellet through the main hopper and C30B powder through the side feeder. The content of Cloisite 30B in the masterbatch was approximately 15 wt %. The prepared pellets (masterbatch) were then dried in a vacuum oven at 60°C for 12 h to remove any possible residual water. The inorganic content of clay in the master batch was determined by burning a few grams of sample in a furnace at 800°C. The test was performed for three different samples and good reproducibility in the results of inorganic content was observed, indicating a well-mixed masterbatch (inorganic content, 15 ± 1 wt %). The prepared master batch was then used to prepare nanocomposites based on PLA/PBSA blends. PLA, PBSA, and the masterbatch, all in the form of pellets, were first hand mixed in a plastic container. The hand-mixed samples were then processed using the same twin-screw extruder. Nanocomposites were prepared at a single-clay concentration (3 wt %). All extrusion processes were performed at the screw speed of 100 rpm. The following temperature profile (from the feeder to the die) was used in the extrusion process: 170, 175, 175, 180, 180, 180, 180, and 175°C. To cover the whole concentration range, pure PLA and PBSA were also processed under the same processing conditions.

Morphological Characterization

The samples for scanning electron microscopic (SEM) measurements were prepared by cryofracture in liquid nitrogen of strands obtained in the extrusion process. The cryofractured samples were then coated with gold–palladium vapor deposit for a period of 30 s. The morphology of the blends was observed by field emission scanning electron microscopy (FE-SEM, Hitachi S-4700) operated at 2 kV. The nanoscale morphology of the ternary nanocomposite was also examined by high-resolution transmission electron microscopy (TEM, Philips, CM200), operated at an accelerating voltage of 200 kV. For TEM measurements, ultrathin sections were prepared by cryogenic ultramicrotome, operated at $T = -100$°C with a diamond knife. Disk-shape samples of approximately 2 mm thickness were used for X-ray diffraction (XRD) measurements. XRD experiments were carried out using a Bruker Advanced X-ray machine (Bruker AXS, Madison, WI) equipped with an area detector diffraction system. The area detector diffraction system in XRD measurements makes it possible to cover a larger area of the sample, leading to a precise measurement. The scans were performed in a one-frame measurement for a period of 60 s. This procedure covers 2θ ranges from 0.5 to 28°. To have a reference, the XRD test was also performed for the pure components.

Rheological Measurements

The transient elongational viscosity was measured using a SER Universal Testing Platform (Xpansion Instruments LLC) in combination with Anton Paar Physica MCR 501 rotational rheometer. Transient stress growth experiments were carried out over a range of Hencky strain rates from 0.5 to 8 s^{-1} and the test temperature was kept at 180°C. The detailed operating principle of the SER Universal Testing Platform can be found elsewhere.[22,23] To prepare the specimen for the test, the pellets obtained during the extrusion process were molded into rectangular sheets (with the nominal thickness of 1 mm) by compression molding, using a flat window frame mold. Compression molding was carried out at 5 MPa and 180°C for a period of 15 min (5-min preheating, 5-min heating under pressure, and 5-min cooling under pressure). A dual blade cutter with a fixed gap spacer was then used for cutting a rectangular specimen with fixed width. The ultimate approximate dimension of the test specimen was 17 mm in length, 12.7 mm in width, and

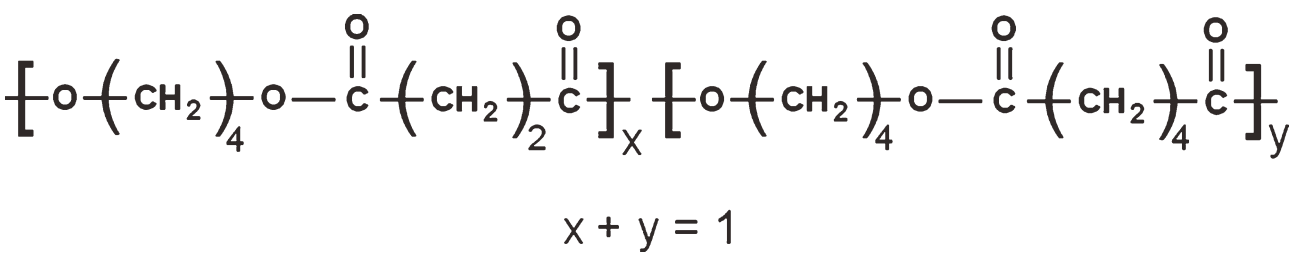

Scheme 2. The chemical structure of PBSA.

Applied Polymer SCIENCE

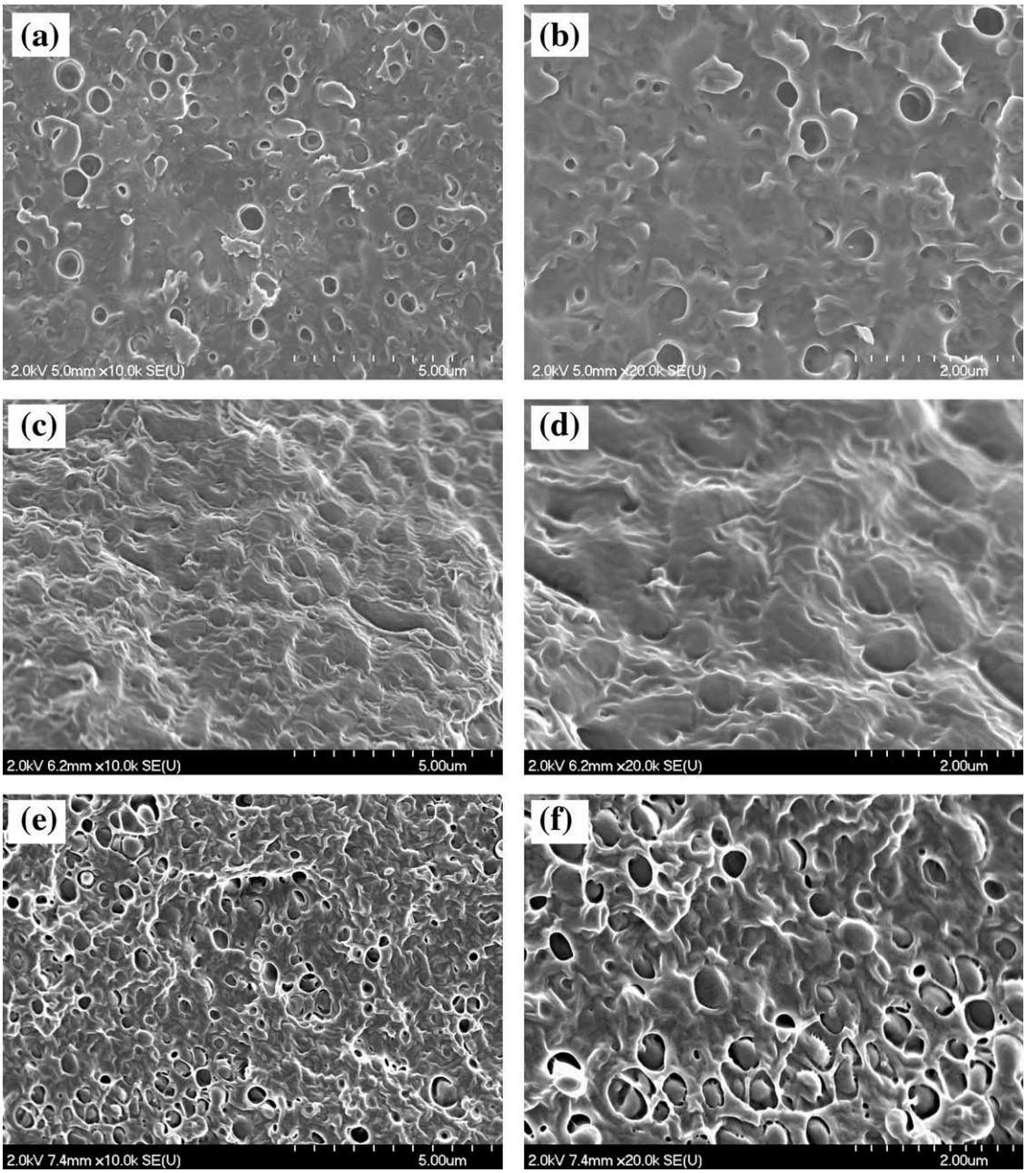

Figure 1. FE-SEM images of PLA/PBSA binary blends (a,b) PLA/PBSA: 75/25, (c,d) PLA/PBSA: 50/50, and (e,f) PLA/PBSA: 25/75.

0.8–01 mm in thickness. It is worth mentioning that the loading procedure of the sample (i.e., opening the door of the oven chamber, fixing the sample onto the SER fixture, and finally closing the door of the oven chamber) and the waiting period prior to starting a test have substantial influence on the accuracy and reproducibility of the extensional experiment. More specifically, the sample has to be loaded in the fixture as fast as possible, to minimize the temperature drop of the oven chamber. Furthermore, to avoid the sagging of the sample, the test has to be started as soon as the sample reaches its equilibrium temperature. In the present study, the loading procedure took about 30 s and the sample was allowed to reach its equilibrium temperature for a period of about 2 min.

Dynamic oscillatory shear measurements were performed using a stress-controlled rheometer (Physica MCR 501, Anton Paar) with parallel plate configuration at 180°C. A disk-shape specimen (25 mm in diameter and 2 mm in thickness) was first placed in the parallel plate fixture and left for 10 min. The gap was then adjusted to 1.3 mm by gradually squeezing the sample. Dynamic frequency sweep experiments were then performed in the linear viscoelastic region over a range of frequency from 0.25 to 100 rad/s. Disk-shape specimens were prepared using a compression molding machine operated at 5 MPa and 180°C for a period of 15 min (5-min preheating, 5-min heating under pressure, and 5-min cooling under pressure).

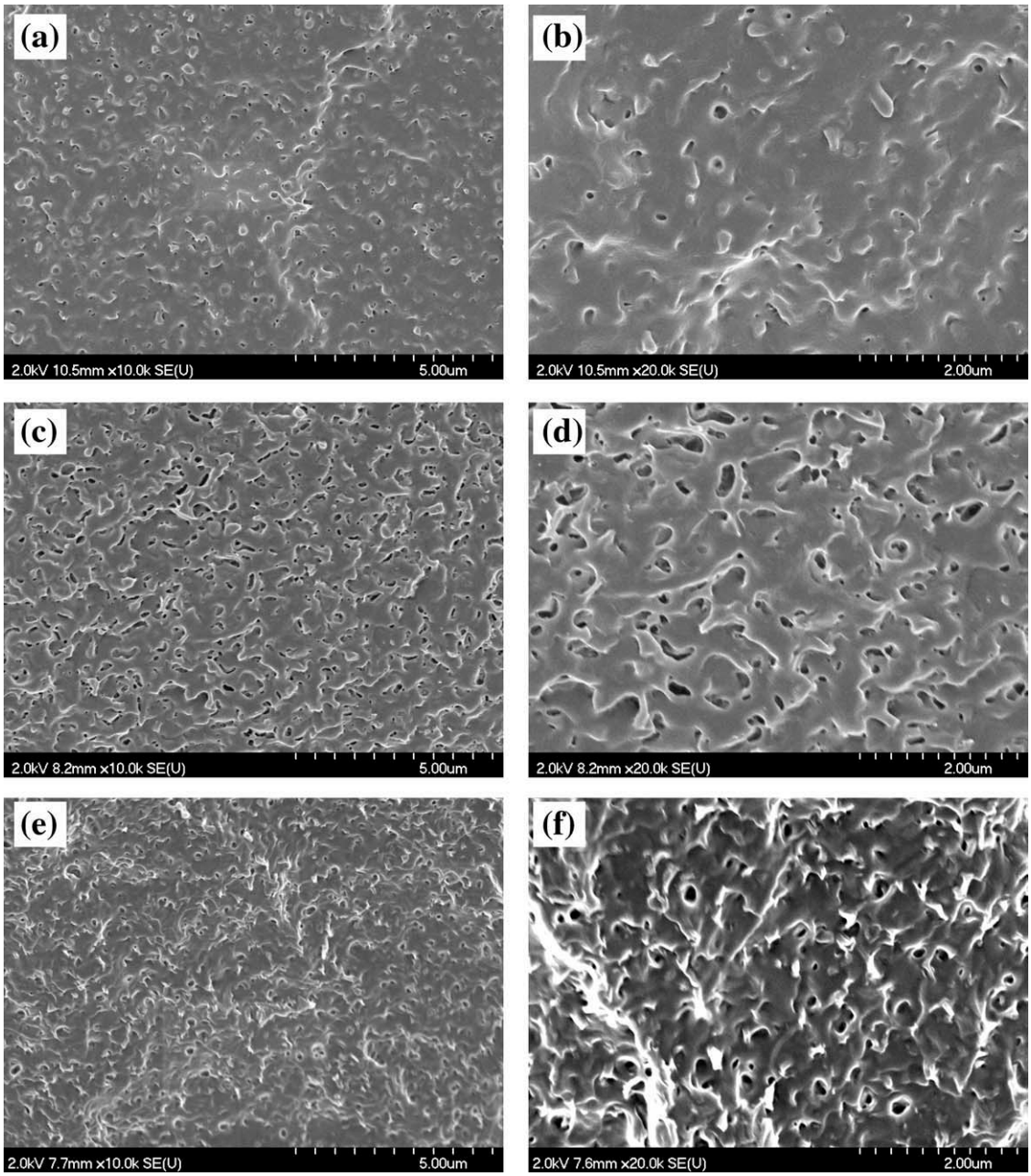

Figure 2. FE-SEM images of PLA/PBSA/Clay ternary nanocomposites at different blend compositions (a,b) PLA/PBSA: 75/25, (c,d), PLA/PBSA: 50/50, and (e,f) PLA/PBSA: 25/75.

RESULTS

Morphology

Figure 1 shows the FE-SEM images of fractured surface of various compositions of PLA/PBSA binary blends. The results show that the phase inversion occurs as PBSA content reaches around 50 wt % PBSA. For blends with PBSA content smaller than 50 wt %, the dispersed phase, PBSA, exhibits droplet morphology with a relatively small mean diameter [Figure 1(a,b)]. A nearly cocontinuous morphology is obtained for the blend containing 50 wt % PBSA [Figure 1(c,d)]. As PBSA content exceeds 50 wt %, PBSA becomes the continuous phase, whereas PLA changes into the dispersed phase [Figure 1(e,f)]. It is now well-established that both the viscosity and the elasticity ratios are important factors influencing the deformation and the size of the dispersed phase during mixing.[12] The mean diameter of the dispersed phase appears to be smaller for the blend containing 75 wt % PBSA than for the blend containing 25 wt % PBSA (compare Figure 1(a) with (e)). This is possibly because the viscosity and the elasticity of PBSA are higher than those of PLA. The higher is the viscosity and the elasticity of the dispersed phase, the more difficult it will be to deform it during mixing.[12] Therefore, PLA droplets in a PBSA matrix deform and break more easily than PBSA droplets in a PLA matrix, leading to smaller droplets for PLA in a PBSA matrix, under the same mixing conditions.

Now, we turn to the morphology of PLA/PBSA/Clay ternary nanocomposites. Figure 2 shows the FE-SEM images of fractured surface of PLA/PBSA/Clay ternary nanocomposites with various blend compositions. In general, the results indicate that incorporation of clay particles reduces the scale of morphological features compared to the corresponding blends. In particular, for blends that exhibit droplet morphology, the mean diameter of the droplets becomes smaller in the presence of clay platelets (compare Figure 1(a,e) with Figure 2(a,e), respectively). Moreover, clay induces a change in morphology from spherical droplet to elongated droplet when PBSA content increases. It can be related to the higher viscosity and elasticity of PBSA phase. In Figure 3, the high magnification images of the ternary nanocomposites with different blend compositions are compared. As shown in Figure 3(a,c), the morphology of the nanocomposites containing 25 and 75 wt % PBSA remains matrix-droplet type morphology. It is believed that clay platelets play the role of compatibilizer and suppress the coalescence, resulting in finer droplet morphology in nanocomposites compared to the corresponding blends. However, for nanocomposite containing 50 wt % PBSA [Figure 3(b)], not only the morphological domains become finer (compare Figure 1(c,d) with Figure 2(c,d)), but also the type of morphology changes from a nearly cocontinuous morphology into an elongated droplet morphology (see also high-magnification image in Figure 3(b)).This may be because the viscosity and the elasticity ratio change in the presence of clay platelets owing to the slightly different affinity of organoclay to PLA and PBSA. Figure 4 shows the TEM images for ternary nanocomposite containing 50 wt % PBSA at three different magnifications. Figure 4(a) shows the typical two-phase structure for ternary nanocomposite in which the dark gray and the light areas correspond to the PBSA and the PLA phases, respectively. TEM images show that clay platelets are well dispersed, at the nanoscale, although some clay tactoids (ordered structure of clay platelets) still remain. The presence of clay tactoids is further confirmed by XRD measurements (Figure 5). Exfoliated clay platelets can be seen in the high-magnification TEM images [Figure 4(b,c)]. As we shall see from the analyses of the interfacial energy data in the **DISCUSSION** section, clay platelets are preferentially located at the phase interface and only small proportion of them are located within the PLA and PBSA phases. We shall return to this issue in the **DISCUSSION** section.

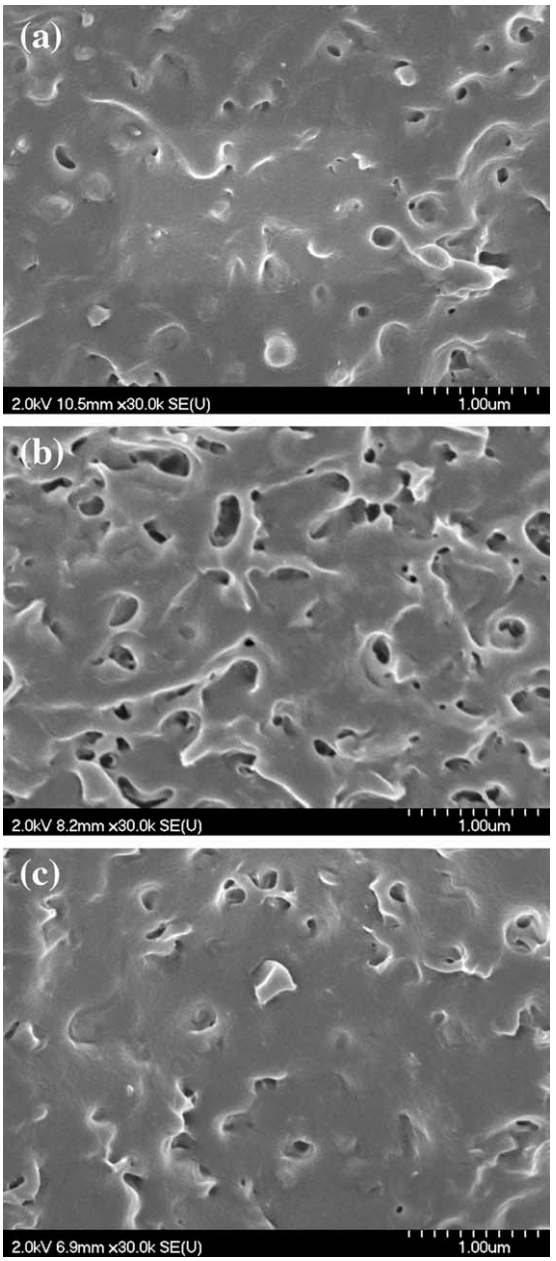

Figure 3. High-magnification FE-SEM images of PLA/PBSA/Clay ternary nanocomposites at different blend compositions (a) PLA/PBSA: 75/25, (b) PLA/PBSA: 50/50, and (c) PLA/PBSA: 25/75.

X-ray Diffraction

Figure 5 shows the XRD patterns of PLA, PBSA, their blends, and their nanocomposites with Cloisite 30B. The XRD pattern of pure PBSA shows three distinct diffraction peaks at about $2\theta = 19.16$, 22.02, and 25.16°. However, pure PLA presents no clear diffraction peaks, an indication of its amorphous structure. It should be noted that the broad peak observed in the XRD pattern of pure PLA is associated with its amorphous phase.[24–26] Figure 5(a) shows that various compositions of the blends present the same diffraction peaks, in terms of position, as pure PBSA. In other words, no noticeable shift in the characteristic diffraction peaks of PBSA is observed when PLA is added. As shown in Figure 5(a), the intensity of the diffraction peaks decreases with an increase of PLA content.

The position, shape, and intensity of the basal reflections of silicate layers in XRD indicate the extent of intercalation in nanocomposites.[6,10,27–29] Figure 5(b) shows the XRD patterns of Cloisite 30B, pure PLA, pure PBSA, and nanocomposites with various blend compositions. Figure 5(b) shows a diffraction peak around $2\theta = 4.6°$ for Cloisite 30B, which shifts to the lower angle ($2\theta = 2.2$–3.15°) for the nanocomposites. This means that the interlayer spacing of clay lamellae increases and polymeric chains penetrate into the clay galleries. The XRD patterns of blends and nanocomposites at two different blend compositions are also compared in Figure 6(a,b) for blends containing 25 and 75 wt % PBSA, respectively. The results of the XRD

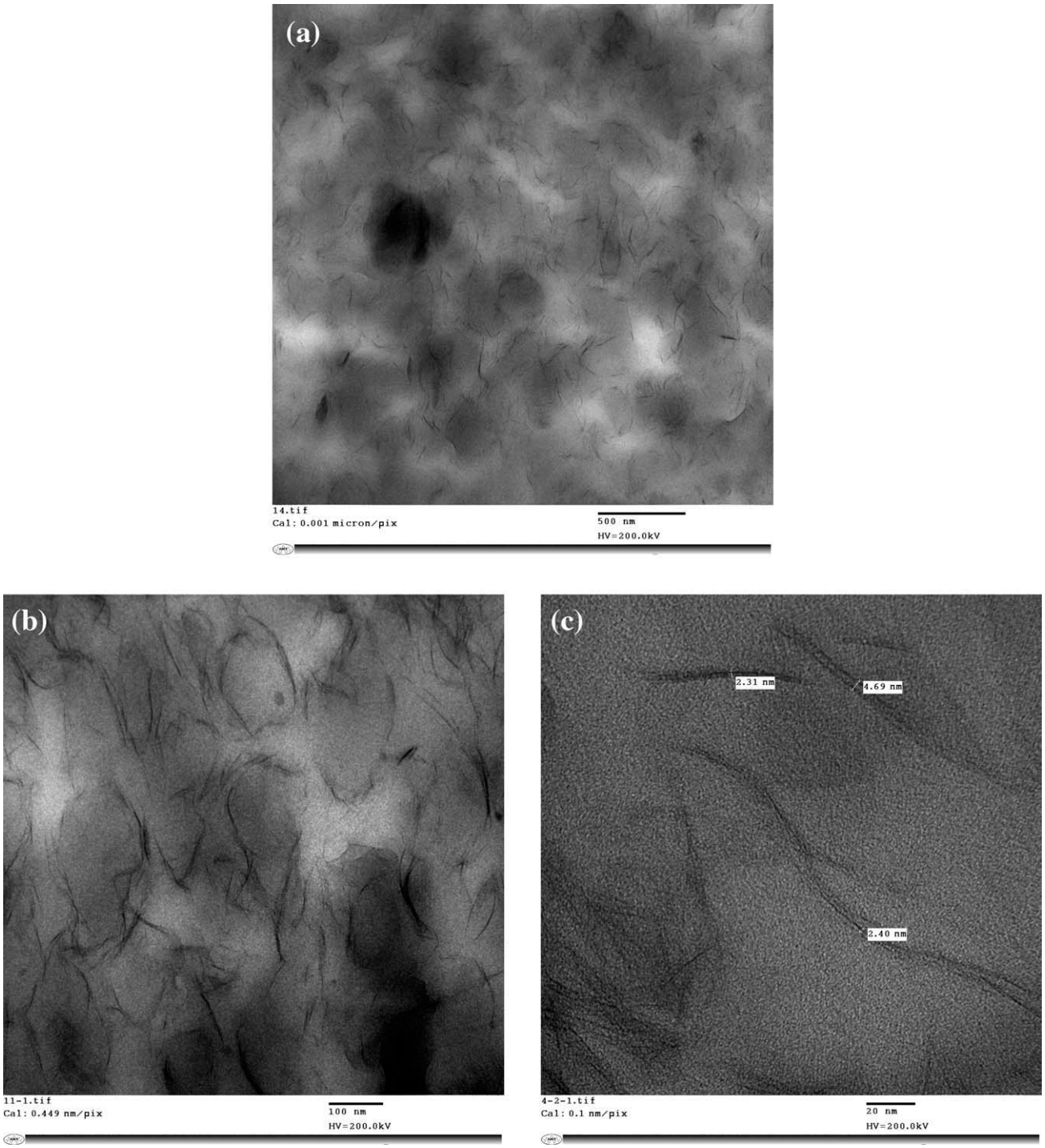

Figure 4. TEM images of PLA/PBSA/Clay ternary nanocomposite containing 50 wt %PBSA at three different magnifications.

observations reveal that the diffraction peak of Cloisite 30B shifts from $2\theta = 4.6$ to 3.15° for the nanocomposite containing 25 wt % PBSA, whereas it shifts from $2\theta = 4.6$ to 2.2° for nanocomposite containing 75 wt % PBSA. Thus, the interlayer spacing of clay lamellae in PLA/PBSA/Clay ternary nanocomposites increases as PBSA content increases. This may be related to the differences in affinity of Cloisite 30B to the blend components, which influences clay localization. The finer droplet size observed in nanocomposites containing 75 wt % PBSA compared to the corresponding morphology in nanocomposite containing 25 wt % PBSA also confirms this observation. The shift of the diffraction peak of Cloisite 30B to the lower angle at 75 wt % PBSA is in line with the good dispersion observed in TEM images. It should be noted that a diffraction peak is

Applied Polymer SCIENCE

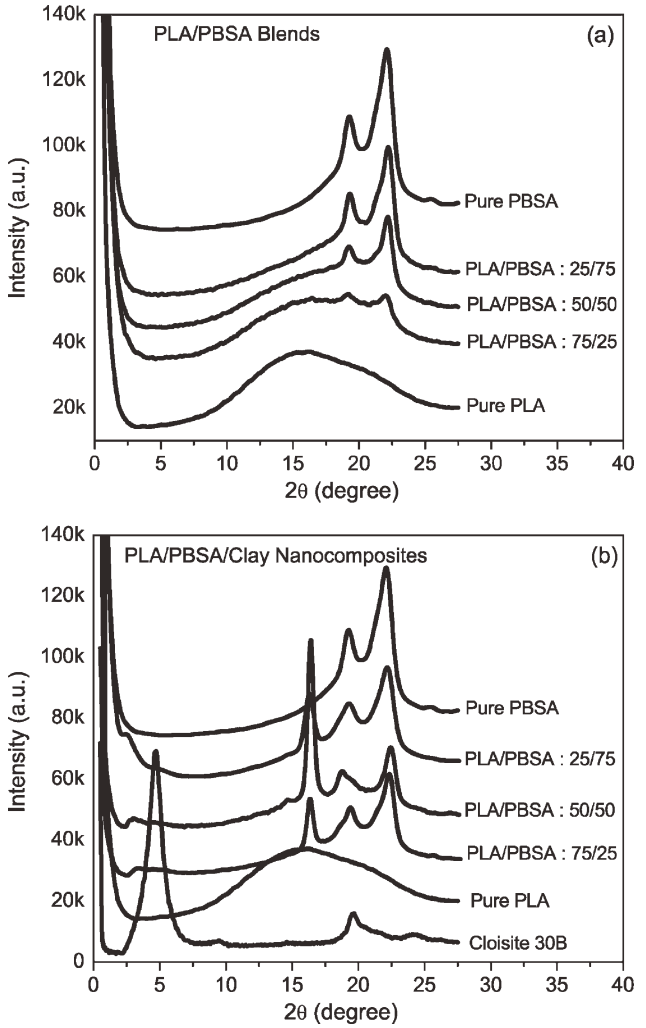

Figure 5. XRD patterns (a) PLA/PBSA binary blends and (b) PLA/PBSA/Clay ternary nanocomposites.

observed at about $2\theta = 16.2°$ for nanocomposite, which is not present for the blend. This is a diffraction peak of Cloisite 30B which is shifted from $2\theta = 19.4$ to $16.2°$ for nanocomposite.

Rheology

Extensional Flow. In many polymer processes such as film blowing, fiber spinning, thermoforming, blow molding, foaming, etc., the major mode of the deformation is elongational flow. Moreover, the extensional flows are considered as strong flows, which can significantly orient macromolecular chains, droplets in polymer blends, and anisotropic particles in polymer nanocomposites. These orientations will eventually influence the properties of the end-use products. Consequently, a comprehensive knowledge of the elongational flow behavior is crucial for the optimization product composition, processing conditions, and product properties.[30–32]

The results of the extensional (elongational) melt rheology experiments for pure PBSA and pure PLA are shown in Figure 7. It should be noted that for the sake of clarity, the elongational viscosity of PBSA was shifted one decade upward. The uniaxial elongational tests were performed at strain rates $>0.5\ s^{-1}$, where an accurate signal can be obtained from the transducer. Figure 7 shows strong strain hardening behavior for pure PBSA at strain rate as low as $0.5\ s^{-1}$. It is possible that strain hardening could start at even a lower strain rate. However, the measurement could not be obtained with the existing measurement system, owing to the transducer sensitivity limitations. The results of the elongational test for pure PLA, on the other hand, show no strain hardening in the entire range of applied strain rates. The highly linear structure of PLA is responsible for its weak or no strain hardening behavior under uniaxial extensional flow. Thus, PBSA was chosen for the applications of interest to take advantage of its strong strain hardening behavior, which should also be reflected by enhanced melt strength in PLA/PBSA blends and PLA/PBSA/Clay nanocomposites.

Figure 8 shows plots of elongational viscosity as a function of time for various compositions of the blend. Again, for the sake

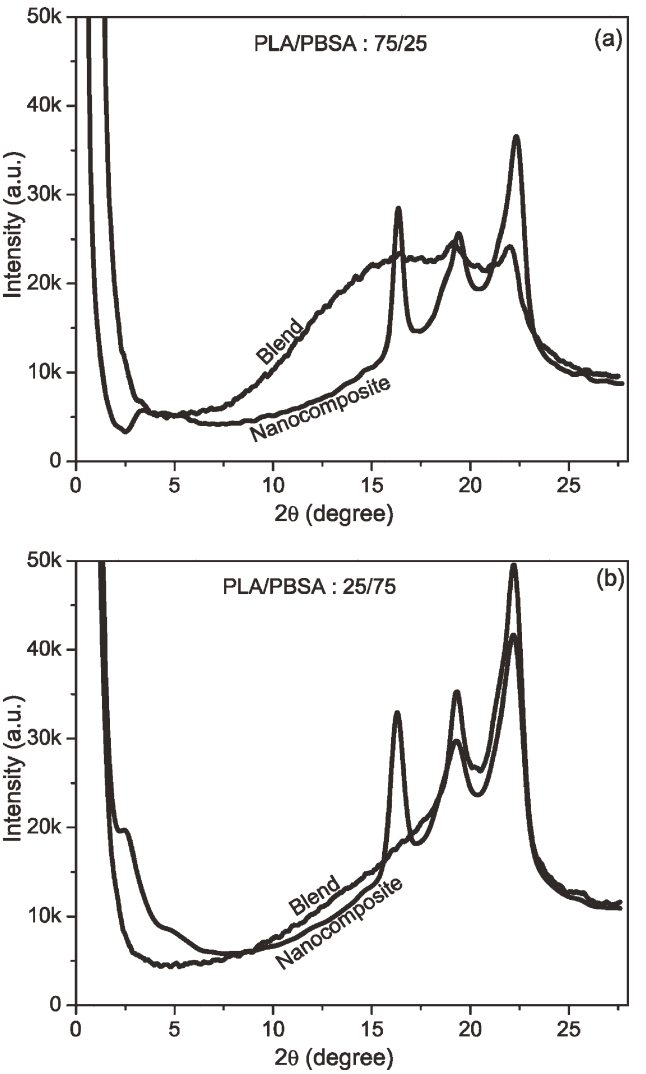

Figure 6. Comparison between XRD patterns of PLA/PBSA binary blend and PLA/PBSA/Clay ternary nanocomposites (a) PLA/PBSA: 75/25 and (b) PLA/PBSA: 25/75.

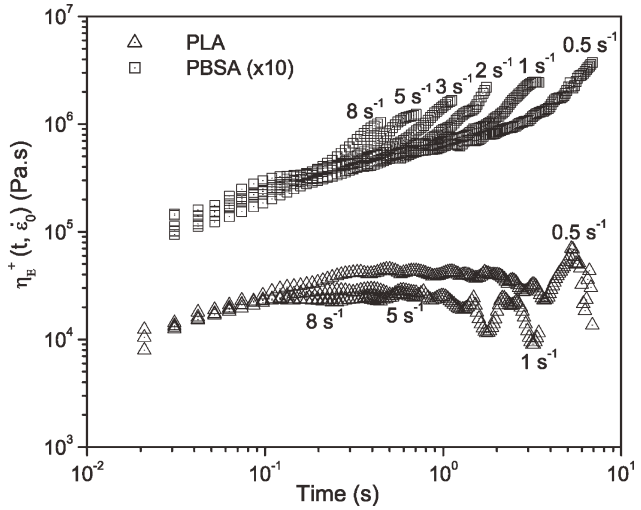

Figure 7. Uniaxial elongational viscosity at various strain rates for pure PLA and pure PBSA.

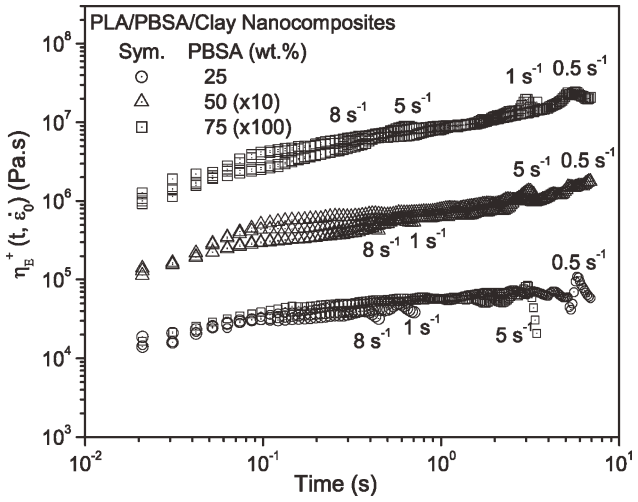

Figure 9. Uniaxial elongational viscosity at various strain rates for different compositions of PLA/PBSA/Clay ternary nanocomposites.

of the clarity, the elongational viscosity of the blends was shifted one and two decades upward for the blends with 50 and 75 wt % PBSA, respectively. It is seen that the incorporation of PBSA into PLA imparts strain hardening behavior to the blends. The blend containing 25 wt % PBSA exhibits weak strain hardening behavior, whereas blends with high PBSA content exhibit well-defined strain hardening behavior which becomes stronger as PBSA content increases (e.g., blends containing 50 and 75 wt % PBSA).

The transient elongational viscosity of PLA/PBSA/Clay ternary nanocomposites with different blend compositions is shown in Figure 9. Again, for the sake of the clarity, the elongational viscosity of the nanocomposites was shifted one and two decades upward for the nanocomposite based on 50 and 75 wt % PBSA, respectively. Again, in Figure 9, no clear strain hardening behavior is observed for nanocomposite based on 25 wt % PBSA.

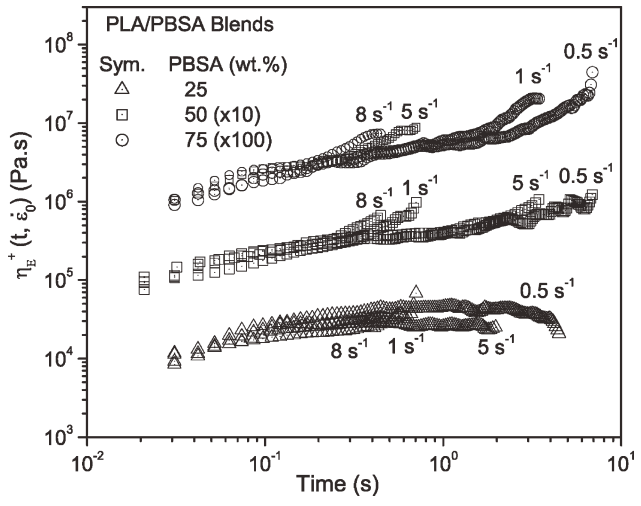

Figure 8. Uniaxial elongational viscosity at various strain rates for different compositions of PLA/PBSA blends.

However, nanocomposites that have higher PBSA content exhibit strain hardening behavior.

The effect of PBSA content on the uniaxial elongational viscosity at a strain rate of 8 s^{-1} is shown in Figure 10(a,b) for blends and nanocomposites, respectively. The results show that the strain hardening becomes more pronounced as PBSA content increases.

Comparison between the transient elongational viscosity of binary blends and the ternary nanocomposites containing 50 wt % PBSA is shown in Figure 11. Two different strain rates are employed for this comparison. Figure 11(a,b) shows that the elongational viscosities of the nanocomposite are higher than those of the blend at small Hencky strain. However, the inverse is observed as the Hencky strain increases. In other words, at the beginning of the transient elongational test, when the strain is small, the values of the elongational viscosities of the blend are smaller than those of the nanocomposites. As the deformation increases with time, the elongational viscosity of the blend becomes larger than that of the nanocomposite. This behavior is observed for all blends and nanocomposites reported in this study, regardless of the composition of the blends.

To elucidate the effect of PBSA content on the strain hardening behavior of the binary blends and ternary nanocomposites, a nonlinear parameter λ_n is defined as follows[33]:

$$\lambda_n = \eta_{E,\text{nonlinear}}/\eta_{E,\text{linear}}$$

in which $\eta_{E,\text{linear}}$ and $\eta_{E,\text{nonlinear}}$ are the elongational viscosities in the short time region and the long time region, respectively.

At a given strain rate, the slope of log λ_n versus Hencky strain defines a measure of the strain hardening intensity. The plots of log λ_n versus Hencky strain at strain rate of 8 s^{-1} are shown in Figure 12(a,b) for binary blends and ternary nanocomposites, respectively. The slopes of the corresponding curves as a function of PBSA content are also shown in Figure 13(a,b). It is found that the strain hardening intensity of the blends increases

Applied Polymer SCIENCE

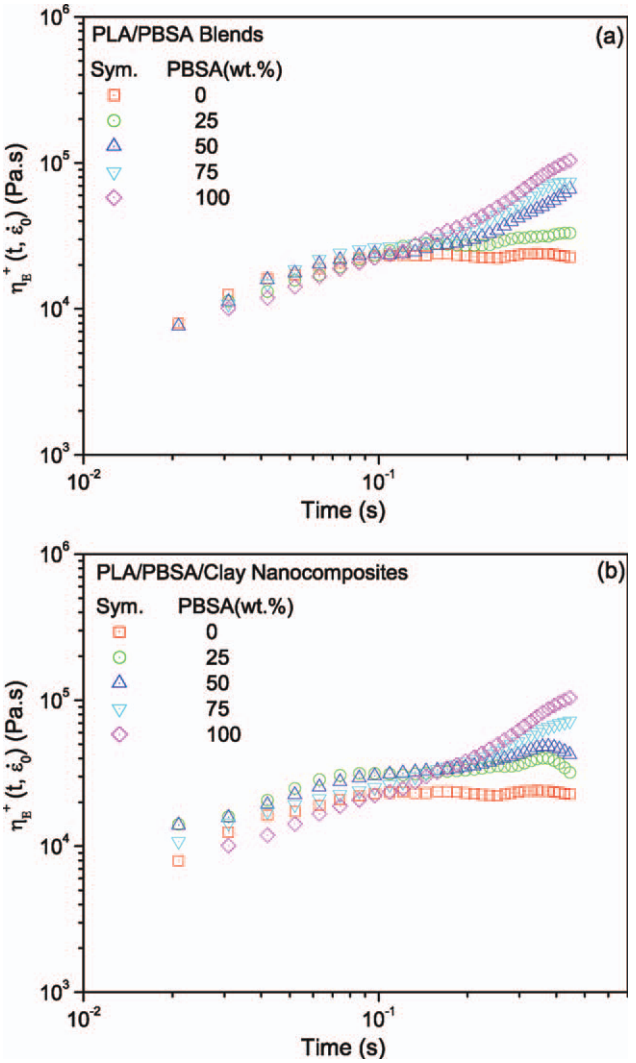

Figure 10. Effect of PBSA content on the uniaxial elongational viscosity at strain rate of 8 s^{-1} (a) PLA/PBSA binary blends and (b) PLA/PBSA/Clay ternary nanocomposite. [Color figure can be viewed in the online issue, which is available at wileyonlinelibrary.com.]

monotonically at low PBSA content. However, a significant increase in the strain hardening intensity is observed at high PBSA content. The same behavior is observed for ternary nanocomposites. However, the intensity of strain hardening for the nanocomposites is smaller than that of the corresponding blends. It can be concluded that the blending of PLA with PBSA as well as the preparation of their nanocomposites would be an effective method for the enhancement of the strain hardening behavior of PLA.

Oscillatory Shear Flow. The results of dynamic frequency sweep test for the blends along with their pure components are shown in Figure 14. The results include complex viscosity (η^*) and storage modulus (G'). Figure 14(a) shows that pure PLA exhibits a clear Newtonian plateau at low frequency, in the measured frequency region, followed by a decrease in complex viscosity at higher frequencies. However, the complex viscosity of pure PBSA does not show a Newtonian plateau, at least in the frequency range investigated in this study. At low frequency, the complex viscosity of pure PBSA is almost five times greater than that of pure PLA. At high frequency, on the other hand, the complex viscosity of pure PBSA becomes comparable to that of pure PLA. The results of Figure 14(a) indicate that at low frequencies, the complex viscosity of the blend increases with increasing PBSA content, except for the blend containing 25 wt % PBSA, where no significant change is observed in its complex viscosity. The storage modulus of the blends along with that of pure components is shown in Figure 14(b). It is found that G' of the blends increases with the increase of PBSA content. As G' is a measure of the elasticity of the system, it can be concluded that the elasticity of PLA/PBSA blends increases with the introduction of PBSA. This is possibly because the highly flexible molecule of PBSA enhances the formation of entanglements in PLA/PBSA blends.

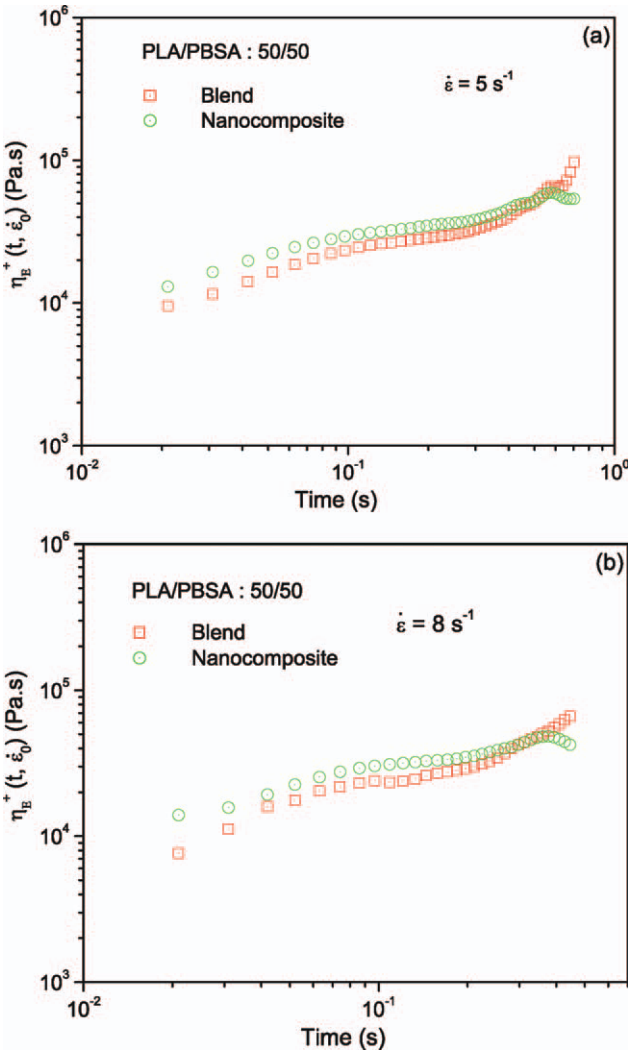

Figure 11. Comparison between uniaxial elongational viscosity of blend and its corresponding nanocomposite with 50 wt %PBSA (a) at strain rate of 5 s^{-1} (b) at strain rate of 8 s^{-1}. [Color figure can be viewed in the online issue, which is available at wileyonlinelibrary.com.]

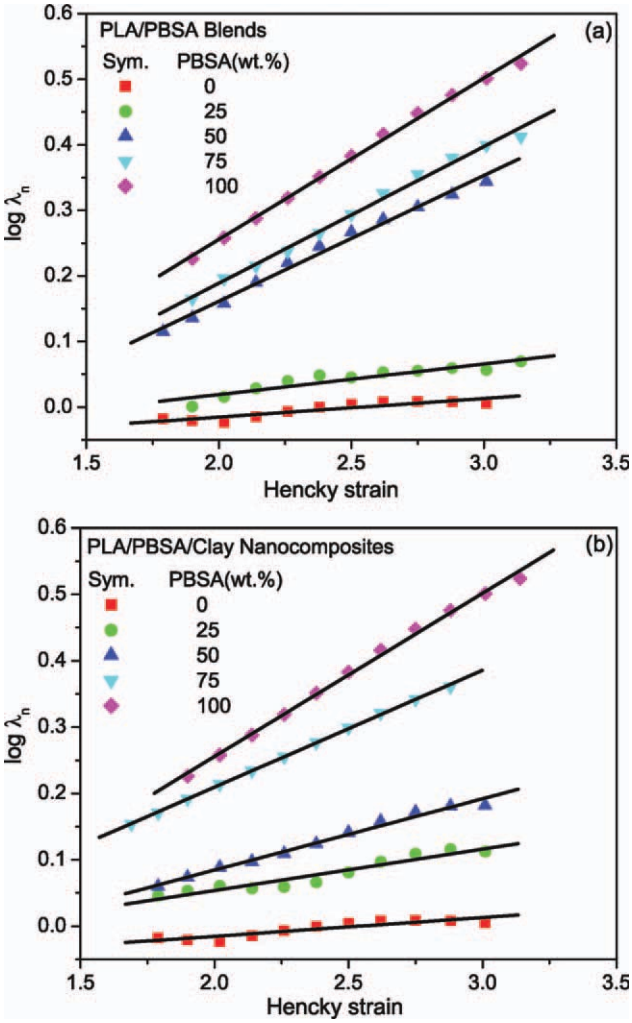

Figure 12. Plot of log λ_n versus Hencky strain at strain rate of 8 s^{-1} (a) PLA/PBSA binary blends and (b) PLA/PBSA/Clay ternary nanocomposite. [Color figure can be viewed in the online issue, which is available at wileyonlinelibrary.com.]

The complex viscosity and storage modulus of the ternary nanocomposite with different blend compositions are shown in Figure 15(a,b), respectively. The results show that the complex viscosity of the nanocomposites is higher than that of the pure components for the entire range of the frequency, except for the nanocomposite based on 25 wt % PBSA at low frequencies. Interestingly, the complex viscosity of the nanocomposite based on 50 wt % PBSA is slightly higher than that of the nanocomposite based on 75 wt % PBSA. The results of Figure 15(b) indicate that the storage modulus of the ternary nanocomposite with different blend compositions is also higher than that of the pure components. Again, the storage modulus of the nanocomposite based on 50 wt % PBSA is higher than that of the nanocomposite based on 75 wt % PBSA. More specifically, nanocomposite containing 50 wt % PBSA exhibited pronounced frequency independence of storage modulus in the terminal region. This can be attributed to the good dispersion of clay lamellae, as confirmed by TEM observations.

The so-called Cole–Cole plot (the curve of η'' versus η') is commonly used to examine the structural changes in multicomponent multiphase polymer systems. Cole–Cole plot represents an empirical correlation between η'' and η'. However, the modified Cole–Cole plot (the curve of log G' versus log G'') has a base of molecular viscoelasticity theory.[34] The modified Cole–Cole plots were widely used for the evaluation of the structural changes in filled polymer system at a fixed temperature.[34–36] The modified Cole–Cole plots for binary blends and ternary nanocomposites are shown in Figure 16(a,b), respectively. Figure 16(a) shows that the modified Cole–Cole plots of the blends deviate from those of the pure components. The slope of the log G' versus log G'' plots for the blends is much smaller than that for pure components (slope of the log G' versus log G'': 1.71 for PLA, 1.45 for PBSA, and around 1.2 for blends). This suggests that all PLA/PBSA blends are immiscible, confirming the result of SEM observations.[34] Figure 16(b) shows that the deviation from the pure components becomes more pronounced in ternary nanocomposites. Nonlinear behavior is clearly observed in the

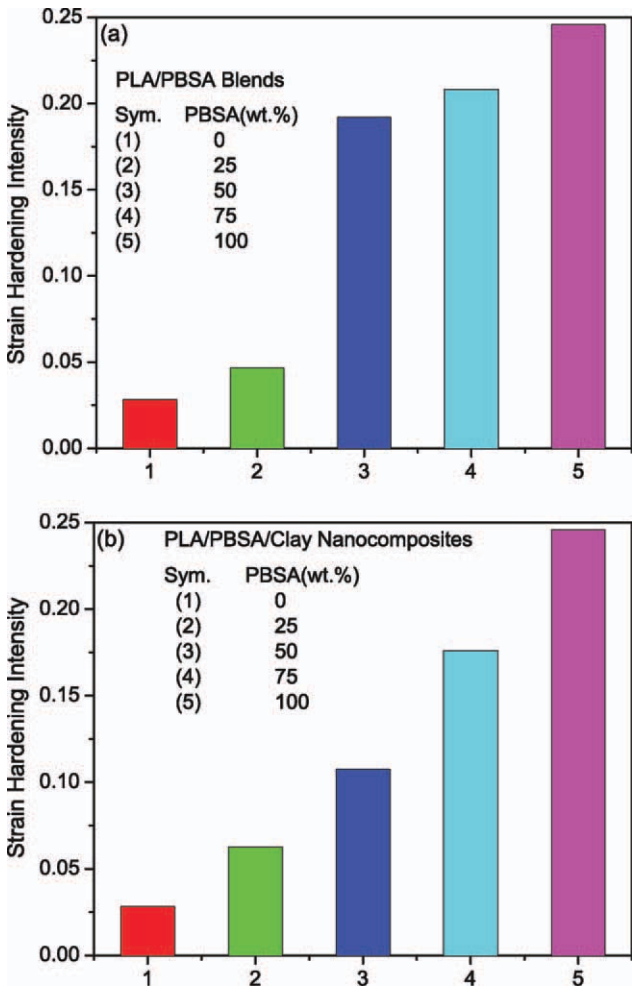

Figure 13. Strain hardening intensity at various blend compositions at strain rate of 8 s^{-1} (a) PLA/PBSA binary blends and (b) PLA/PBSA/Clay ternary nanocomposites. [Color figure can be viewed in the online issue, which is available at wileyonlinelibrary.com.]

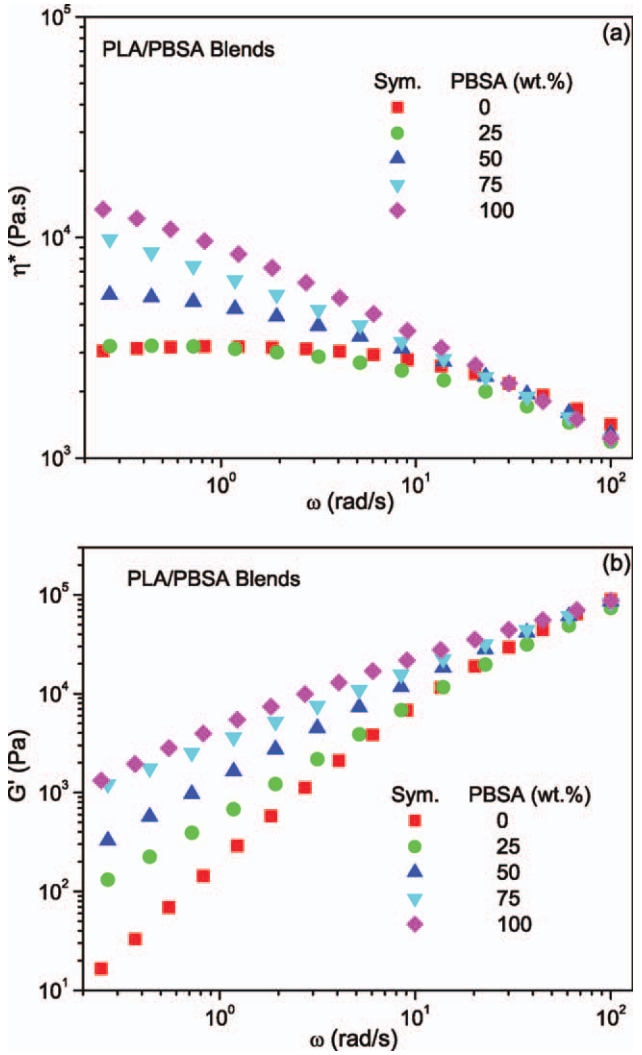

Figure 14. Linear viscoelastic properties of binary PLA/PBSA blends (a) complex viscosity and (b) storage modulus. [Color figure can be viewed in the online issue, which is available at wileyonlinelibrary.com.]

modified Cole–Cole plot of nanocomposite containing 50 wt % of PBSA. The slope of the log G' versus log G'' plots for the nanocomposites is not only smaller than that for pure components but also smaller than that for the blends. The slope changes form 1.2 for PLA/PBSA blends to 0.35 for nanocomposite containing 50 wt % PBSA. These observations reveal an additional structural change in ternary nanocomposites because of the presence of clay platelets.

The complex viscosity of the PLA/PBSA binary blend and the PLA/PBSA/Clay ternary nanocomposite with 25 wt % PBSA are compared in Figure 17. The corresponding storage modulus is also inserted in Figure 17. The results show that the values of G' and η^* for the nanocomposite are greater than those for the blend in the entire range of the frequency. Moreover, the effect of clay platelets is very large at low frequencies. This may be attributed to the presence of plateau in G' and the rising complex viscosity in the low frequency region. Qualitatively, the same behavior is observed for nanocomposites and blends with 50 and 75 wt % of PBSA (Figures 18 and 19). However, the frequency dependence of the storage modulus of nanocomposite with 50 wt % PBSA is weaker than that observed for nanocomposites with 25 and 75 wt % PBSA. Such behavior, known as solid-like behavior, has been reported for both intercalated and exfoliated polymer nanocomposites.[21,37–45]

DISCUSSION

The above observations have shown that strong solid-like behavior is observed for nanocomposites containing 50 wt % PBSA. This behavior is less pronounced for the other ternary nanocomposites. One question remains to be answered. Why do we observe a pronounced solid-like behavior for nanocomposite based on 50 wt % PBSA while the clay concentration is almost the same for all ternary nanocomposites? We suggest the following interpretation:

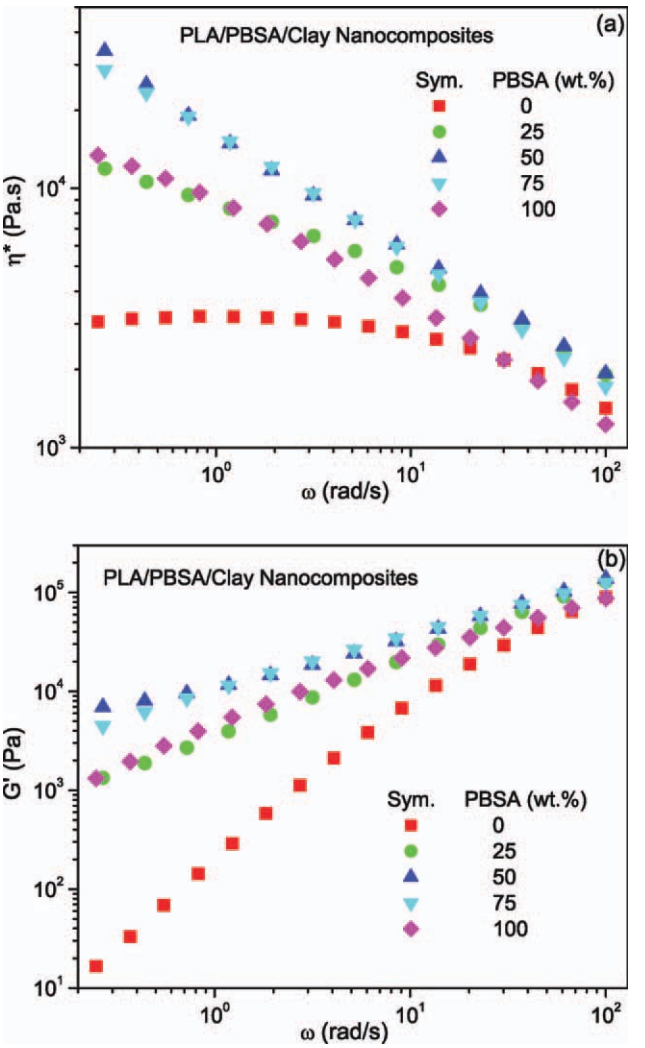

Figure 15. Linear viscoelastic properties of ternary PLA/PBSA/Clay nanocomposites (a) complex viscosity and (b) storage modulus. [Color figure can be viewed in the online issue, which is available at wileyonlinelibrary.com.]

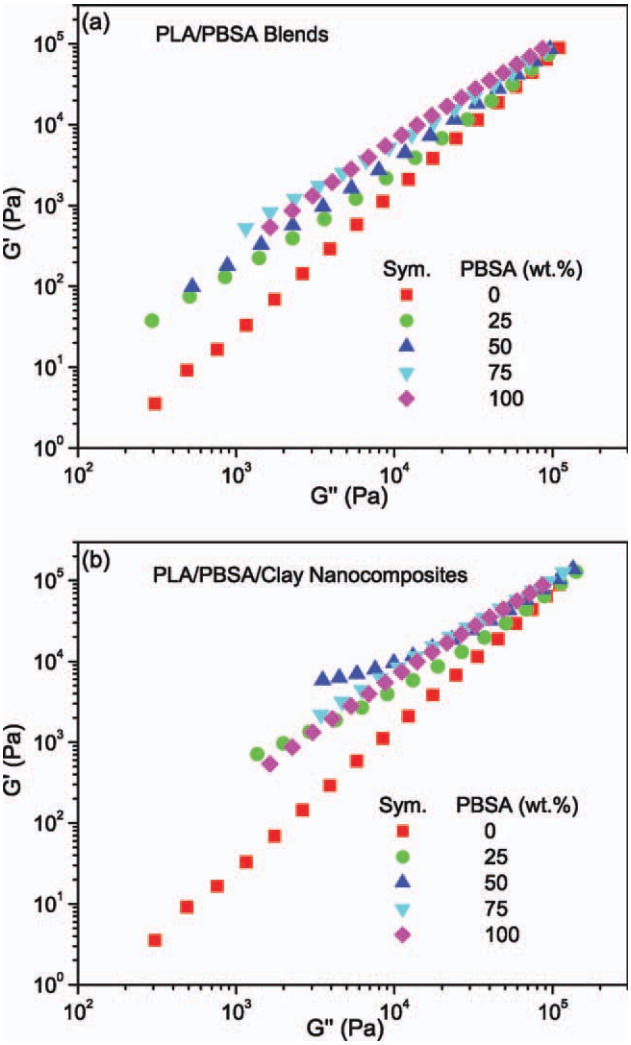

Figure 16. Modified Cole–Cole plot for (a) PLA/PBSA binary blends and (b) PLA/PBSA/Clay ternary nanocomposites. [Color figure can be viewed in the online issue, which is available at wileyonlinelibrary.com.]

It is now well-established that the solid-like behavior observed in the linear rheology of polymer nanocomposites is owing to the formation of network-like structure in the suspension.[21,37–45] The network-like structure is more obvious at lower frequencies (or equivalently at large time scale) and less so at higher frequencies (or equivalently at small time scale). However, the nature of this network-like structure has not been well understood. It may depend on particle–particle and polymer–particle interactions which vary from one polymeric system to the other. Polymer–particle and particle–particle interactions are expected to play an important role in the rheology of nanocomposites where the particle number density is quite high. In particular, particle–particle interactions are expected to become important where the particles are highly anisotropic such as the clay platelets. Above the percolation threshold, the proximity of the particles and the topological constraints are responsible for the formation of the network-like structure. This network-like structure is known as particle–particle network-like structure.[21,37–45] Polymer–particle interactions, on the other hand,

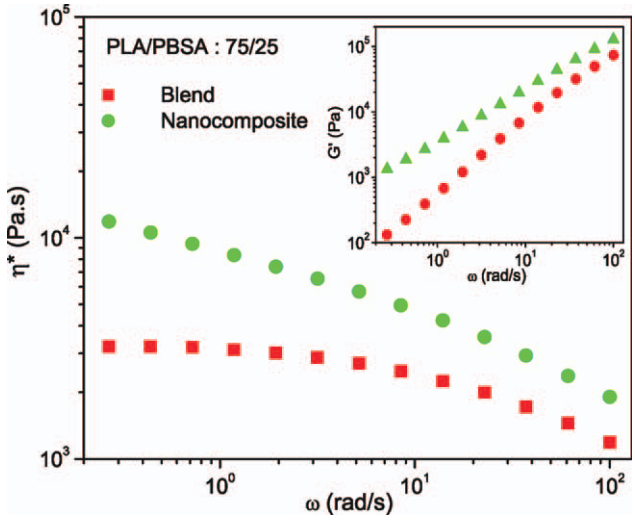

Figure 17. Comparison between complex viscosity and storage modulus (inset) of PLA/PBSA binary blend and PLA/PBSA/Clay ternary nanocomposites with 25 wt %PBSA. [Color figure can be viewed in the online issue, which is available at wileyonlinelibrary.com.]

are anticipated to become important in the formation of the network-like structure when there is a good affinity between polymer chains and particles. This affinity depends on the type and the length of the modifier on the surface of the particles. More specifically, it depends on the interfacial energy between polymer and particle. In such systems, the network-like structure is formed by linking between polymeric chains and particles, even below the percolation threshold. According to Zhang and Archer,[46] even for isolated nanoparticles dispersed in a polymeric host, strong polymer–particle interactions may induce absorption of the polymeric chains on the particles and form network-like structure.[46] This network-like structure is recognized as polymer–particle network-like structure.

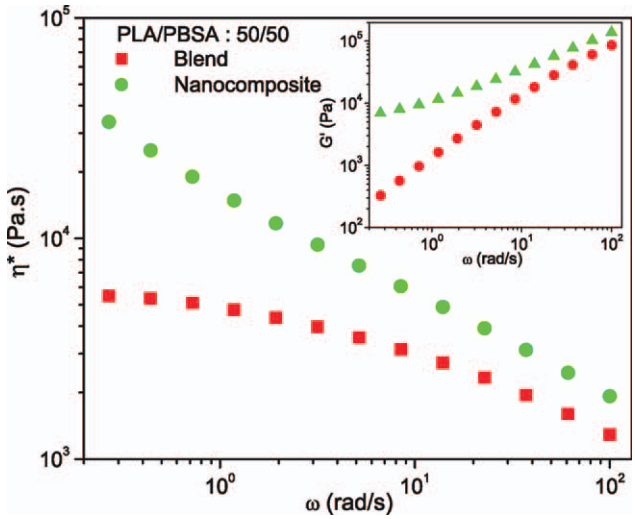

Figure 18. Comparison between complex viscosity and storage modulus (inset) of PLA/PBSA binary blend and PLA/PBSA/Clay ternary nanocomposites with 50 wt %PBSA. [Color figure can be viewed in the online issue, which is available at wileyonlinelibrary.com.]

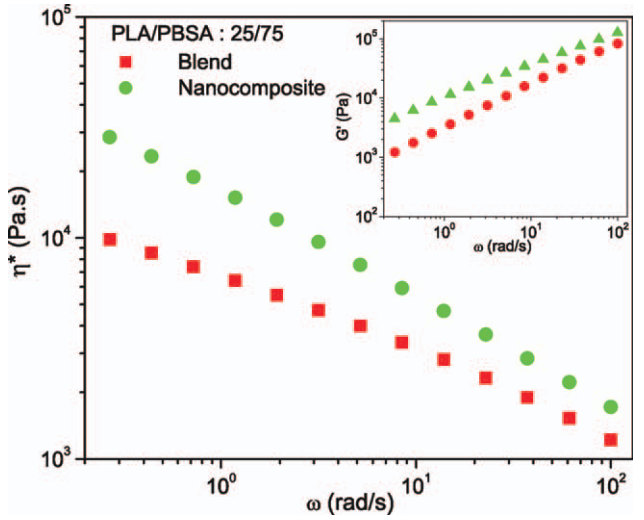

Figure 19. Comparison between complex viscosity and storage modulus (inset) of PLA/PBSA binary blend and PLA/PBSA/Clay ternary nanocomposites with 75 wt %PBSA. [Color figure can be viewed in the online issue, which is available at wileyonlinelibrary.com.]

In the ternary nanocomposites investigated in this study, the solid-like behavior observed in the low-frequency region (i.e., low-frequency plateau in storage modulus, Figures 17–19) confirms the existence of such a network-like structure. The intensity of the network-like structure depends on the morphology of the blends (droplet or cocontinuous morphology) and the selective localization behavior of the clay platelets within the ternary nanocomposites.

According to Young's equation, the selective localization behavior of filler in ternary systems can be evaluated by estimating the wetting coefficient ω_a as follows[16,47,48]:

$$\omega_a = \frac{\sigma_{\text{filler}-B} - \sigma_{\text{filler}-A}}{\sigma_{A-B}}$$

where $\sigma_{\text{filler}\ -\ A}$ and $\sigma_{\text{filler}\ -\ B}$ are the interfacial energy between filler and component A and filler and component B, respectively. $\sigma_{A\ -\ B}$ is the interfacial energy between component A and component B. If the wetting coefficient is higher than 1 ($\omega_a > 1$), the filler is located in phase A. The filler is located in phase B, if the wetting coefficient is lower than -1 ($\omega_a < -1$). When the wetting coefficient is between 1 and -1 ($-1 < \omega_a < 1$), the filler is preferentially located at the interface between the two blend components.[16]

According to the geometric-mean equation, the interfacial energy between two components γ_{AB} can be calculated as follows[16,47,48]:

$$\gamma_{AB} = \gamma_A + \gamma_B - 2[(\gamma_A^d \gamma_B^d)^{1/2} + (\gamma_A^p \gamma_B^p)^{1/2}]$$

where γ_A and γ_B are surface energy of the components A and B, and γ_A^d and γ_A^p are the dispersive and the polar portions of the surface energy, respectively.

The literature values of the surface energies of PLA, PBSA, and Cloisite 30B (Table I) are used for the calculation of the interfacial energies for pairs of PLA/PBSA, PLA/C30B, and PBSA/C30B.[16,49,50] The geometric-mean equation is used for this calculation and the data are summarized in Table I. The data in Table I are then used to calculate the wetting coefficient according to Young's equation. The calculated wetting coefficient for PLA/PBSA/Clay ternary nanocomposites is -0.72, which means that clay platelets are mainly located at the phase interface, with small amounts located within the PLA and PBSA phases.

The results of FE-SEM images show that for blends with droplet morphology (e.g., blends containing 25 and 75 wt % PBSA) the type of the morphology of the resultant nanocomposites remains unchanged. In other words, droplet morphology is also observed for nanocomposites containing 25 and 75 wt% PBSA. However, for blend containing 50 wt % PBSA, where the morphology is nearly cocontinuous, incorporation of clay platelets transfers the morphology from cocontinuous to very fine elongated droplet morphology. Therefore, the amount of interface between the dispersed phase and the continuous phase (i.e., interfacial area) for nanocomposite containing 50 wt % PBSA is much higher than that for nanocomposites containing 25 and 75 wt % PBSA. This is basically because the number of droplets is much higher for nanocomposites containing 50 wt % PBSA than those for nanocomposites containing 25 PBSA and 75 wt % PBSA. As for PLA/PBSA/Clay ternary nanocomposites clay platelets are mainly located at the phase interface, higher interfacial area in nanocomposite containing 50 wt % PBSA makes it possible to locate more clay platelets at the phase interface. Higher amounts of clay platelets at the phase interface increase the chance for the formation of polymer–particle and particle–particle network-like structure, which in turn lead to the strong solid-like behavior in nanocomposites containing 50 wt % PBSA. Such a network-like structure is also formed in nanocomposites containing 25 and 75 wt % PBSA. However, its intensity is lower than that observed for nanocomposite containing 50 wt % PBSA.

Table I. Surface Energies for PLA, PBSA, and Cloisite 30B and Interfacial Energies for Pairs of PLA/PBSA, PLA/C30B, and PBSA/C30B Calculated from Geometric-Mean Equation

	Surface energy (mJ/m^2)					
Sample	γ^d	γ^p	γ	Sample A	Sample B	Interfacialenergy, γ_{AB} (mJ/m^2)
PLA	37	13	50	PLA	PBSA	−0.75
PBSA	43	14	56	PLA	Cloisite 30B	1.82
Cloisite 30B	22.4	12.6	35	PBSA	Cloisite 30B	2.36

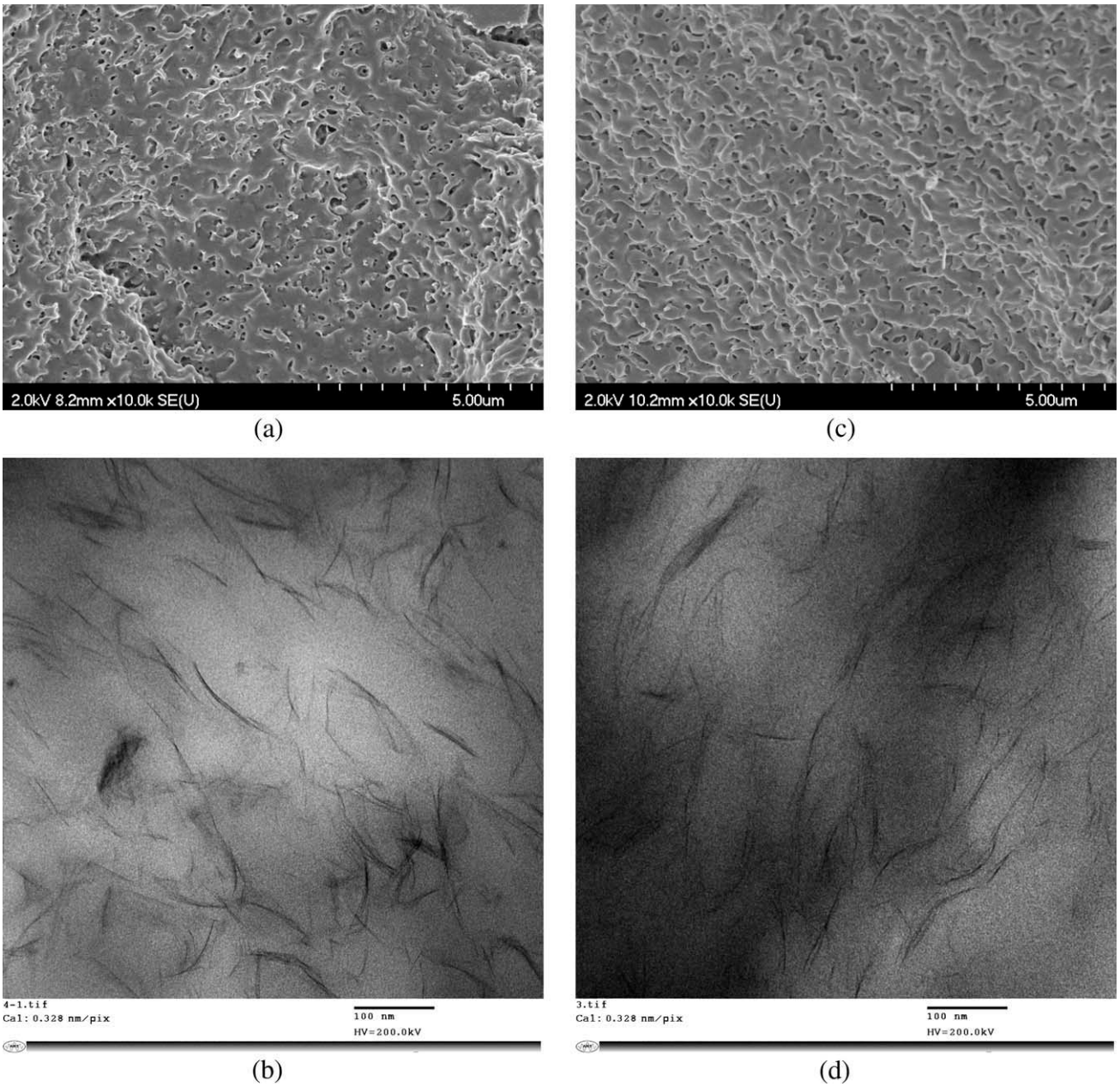

Figure 20. FE-SEM and TEM images of PLA/PBSA/Clay ternary nanocomposite containing 50 wt % PBSA (a,b) before elongational viscosity measurement and (c,d) after elongational viscosity measurement at the strain rate of 8 s^{-1}.

As we discussed in the Extensional Flow section, elongational viscosities of the nanocomposite are higher than those of the blend at small Hencky strain. However, the inverse is observed as the Hencky strain increases. As mentioned above, a network-like structure is formed in ternary nanocomposites, which originates from polymer–particle and particle–particle interactions. Such a network-like structure is not present in binary blends. When the binary blends are subjected to elongational stresses, the stretching of the polymeric chains and the stretching of the interface determine the response to the elongational flow field. However, when the ternary nanocomposites are subjected to elongational stresses, in addition to the stretching of the polymeric chains and the interface, the stretching of the network-like structure also contributes to the response to elongational flow field. At small deformation (or equivalently at short-time scale), the network-like structures in ternary nanocomposite are responsible for the higher elongational viscosity. However, at longer time scale (or equivalently at larger deformation), the network-like structures are destroyed and clay platelets are oriented in the stretching direction. To observe the orientation of clay platelets in nanocomposites, at the end of the elongational tests, the samples were quickly cooled down using compressed air and cryofractured in liquid nitrogen. Figure 20 shows the FE-SEM and TEM images of PLA/PBSA/Clay ternary nanocomposite containing 50 wt %PBSA before and after the elongational test at strain rate of 8 s^{-1}. It is seen that the majority of

clay platelets and the droplets are oriented in the direction of stretching [Figure 20(c,d)]. The oriented clay platelets reduce the stress required for a given deformation, leading to the lower elongational viscosity for ternary nanocomposites at longer times. The same type of observation has been reported by Eslami et al.[21] regarding the normal stress difference of polymer nanocomposites in shear flow.

CONCLUSIONS

Elongational flow and linear viscoelastic melt properties of PLA/PBSA binary blends and PLA/PBSA/Clay ternary nanocomposites were investigated. *A* nearly cocontinuous morphology was achieved for blends containing 50 wt % PBSA. As PBSA content reached more than 50 wt %, PBSA became the major phase and PLA changed into the dispersed phase. The incorporation of PBSA into PLA imparted strain hardening behavior to the blends. The blend containing 25 wt % PBSA exhibited weak strain hardening behavior, whereas blends with high PBSA content exhibited well-defined strain hardening behavior which became stronger as PBSA content increased. No clear strain hardening behavior was observed for nanocomposite based on 25 wt % PBSA. However, nanocomposites based on higher PBSA content exhibited strain hardening behavior. It was found that the elongational viscosities of the nanocomposite were higher than those of the blend at small Hencky strain. However, an inverse behavior was observed as Hencky strain increased. At small deformation, the network-like structures in ternary nanocomposite are responsible for the higher elongational viscosity. However, at large deformation, the network-like structures are destroyed, and clay platelets become oriented in the direction of stretching. The oriented clay platelets contribute to the lower elongational viscosity for ternary nanocomposites. The analyses of the interfacial energy data for PLA/PBSA/Clay ternary nanocomposites revealed that clay platelets were preferentially located at the phase interface with small amounts of clay located within the PLA and PBSA phases. For blends containing 50 wt %PBSA, where the morphology was nearly cocontinuous, incorporation of clay platelets changed the morphology from cocontinuous to very fine elongated droplet morphology. Because of the high interfacial area in nanocomposite containing 50 wt % PBSA, large amounts of clay platelets were located at the interface, which in turn increased the chance for the formation of the polymer–particle and particle–particle network-like structures. Such network-like structures are believed to be responsible for the strong solid-like behavior observed in nanocomposite containing 50 wt % PBSA. Finally, the results of this study suggest that the addition of PBSA to PLA improves PLA's strain hardening behavior, which makes it more suitable for many polymer-processing operations (e.g., film blowing, blow molding, and fiber spinning).

ACKNOWLEDGMENTS

Hassan Eslami is grateful to the government of Quebec for the two-year award of Fonds québécois de la recherche sur la nature et les technologies (FQRNT) postdoctoral fellowship. The authors also acknowledge the financial support provided by the Natural Sciences and Engineering Research Council (NSERC) of Canada.

REFERENCES

1. Lim, L. T.; Auras, R.; Rubino, M. *Prog. Polym. Sci.* **2008,** *33*, 820.
2. Lee, J.; McCarthy, S. J. *Polym. Environ.* **2009,** *17*, 240.
3. Wang, Y.; Mano, J. F. *J. Appl. Polym. Sci.* **2007,** *105*, 3204.
4. Lee, S.; Lee, J. W. *Korea Aust. Rheol. J.* **2005,** *17*, 71.
5. Li, K.; Peng, J.; Turng, L.-S.; Huang, H.-X. *Adv. Polym. Technol.* **2011,** *30*, 150.
6. Alexandre, M.; Dubois, P. *Mater. Sci. Eng. R Rep.* **2000,** *28*, 1.
7. Ray, S. S.; Bousmina, M. *Polymer* **2005,** *46*, 12430.
8. Ray, S. S.; Bousmina, M.; Okamoto, K. *Macromol. Mater. Eng.* **2005,** *290*, 759.
9. Ray, S. S.; Bousmina, M. *Prog. Mater. Sci.* **2005,** *50*, 962.
10. Ray, S. S.; Okamoto, M. *Prog. Polym. Sci.* **2003,** *28*, 1539.
11. Steeves, D. M.; Farrell, R.; Ratto, J. A. *J. Biobased Mater. Bioenergy,* **2007,** *1*, 94.
12. Huitric, J.; Ville, J.; Mederic, P.; Moan, M.; Aubry, T. *J. Rheol.* **2009,** *53*, 1101.
13. Kumar, M.; Mohanty, S.; Nayak, S. K.; Parvaiz, M. R. *Biores. Technol.* **2010,** *101*, 8406.
14. Ko, S.; Hong, M.; Park, B.; Gupta, R.; Choiand, H.; Bhattacharya, S. *Polym. Bull.* **2009,** *63*, 125.
15. Ko, S. W.; Gupta, R. K.; Bhattacharya, S. N.; Choi, H. *J. Macromol. Mater. Eng.* **2010,** *295*, 320.
16. Wu, D.; Lin, D.; Zhang, J.; Zhou, W.; Zhang, M.; Zhang, Y.; Wang, D.; Lin, B. *Macromol. Chem. Phys.* **2011,** *212*, 613.
17. Hong, J. S.; Namkung, H.; Ahn, K. H.; Lee, S. J.; Kim, C. *Polymer* **2006,** *47*, 3967.
18. Bose, S.; Özdilek, C.; Leys, J.; Seo, J. W.; Wübenhorst, M.; Vermant, J.; Moldenaers, P. *ACS Appl. Mater. Interface* **2010,** *2*, 800.
19. Wang, R. Y.; Wang, S. F.; Zhang, Y. *J. Appl. Polym. Sci.* **2009,** *113*, 3095.
20. Tserki, V.; Philippou, J.; Panayiotou, C. *Proc. Inst. Mech. Eng. N J Nanoeng. Nanosyst.* **2006,** *220*, 71.
21. Eslami, H.; Grmela, M.; Bousmina, M. *J. Rheol.* **2010,** *54*, 539.
22. Sentmanat, M.; Wang, B. N.; McKinley, G. H. *J. Rheol.* **2005,** *49*, 585.
23. Sentmanat, M. L. *Rheol. Acta* **2004,** *43*, 657.
24. Rabiej, S. *Eur. Polym. J.* **1993,** *29*, 625.
25. Ren, M.; Song, J.; Song, C.; Zhang, H.; Sun, X.; Chen, Q.; Zhang, H.; Mo, Z. *J. Polym. Sci. B Polym. Phys.* **2005,** *43*, 3231.
26. Lee, T. H.; Boey, F. Y. C.; Khor, K. A. *Polym. Comp.* **1995,** *16*, 481.
27. Lagaly, G. *Solid State Ionics* **1986,** *22*, 43.
28. LeBaron, P. C.; Wang, Z.; Pinnavaia, T. *J. Appl. Clay Sci.* **1999,** *15*, 11.
29. Giannelis, E. P. *Adv. Mater.* **1996,** *8*, 29.
30. Aho, J.; Rolon-Garrido, V. H.; Syrjala, S.; Wagner, M. H. *Rheol. Acta* **2010,** *49*, 359.

31. Nielsen, J. K.; Hassager, O.; Rasmussen, H. K.; McKinley, G. H. *J. Rheol.* **2009,** *53*, 1327.
32. Wagner, M. H.; Kheirandish, S.; Yamaguchi, M. *Rheol. Acta* **2004,** *44*, 198.
33. Nishioka, A.; Onodera, S.; Koda, T.; Miyata, K.; Furuichi, K.; Kodama, K.; Koyama, K. *Polym. J.* **2009,** *41*, 6.
34. Han, C. D.; Kim, J. K. *Polymer* **1993,** *34*, 2533.
35. Kim, J. Y.; Park, H. S.; Kim, S. H. *J. Appl. Polym. Sci.* **2007,** *103*, 1450.
36. Kwag, H.; Rana, D.; Cho, K.; Rhee, J.; Woo, T.; Lee, B. H.; Choe, S. *Polym. Eng. Sci.* **2000,** *40*, 1672.
37. Eslami, H.; Grmela, M.; Bousmina, M. *Rheol. Acta.* **2009,** *48*, 317.
38. Galgali, G.; Ramesh, C.; Lele, A. *Macromolecules* **2001,** *34*, 852.
39. Krishnamoorti, R.; Giannelis, E. P. *Macromolecules* **1997,** *30*, 4097.
40. Krishnamoorti, R.; Vaia, R. A.; Giannelis, E. P. *Chem. Mater.* **1996,** *8*, 1728.
41. Li, J.; Zhou, C.; Wang, G.; Zhao, D. *J. Appl. Polym. Sci.* **2003,** *89*, 3609.
42. Mobuchon, C.; Carreau, P.; Heuzey, M.-C. *Rheol. Acta* **2007,** *46*, 1045.
43. Ren, J.; Silva, A. S.; Krishnamoorti, R. *Macromolecules* **2000,** *33*, 3739.
44. Solomon, M. J.; Almusallam, A. S.; Seefeldt, K. F.; Somwangthanaroj, A.; Varadan, P. *Macromolecules* **2001,** *34*, 1864.
45. Wu, D.; Zhou, C.; Hong, Z.; Mao, D.; Bian, Z. *Eur. Polym. J.* **2005,** *41*, 2199.
46. Zhang, Q.; Archer, L. A. *Langmuir* **2002,** *18*, 10435.
47. Katada, A.; Buys, Y.; Tominaga, Y.; Asai, S.; Sumita, M. *Colloid Polym. Sci.* **2005,** *284*, 134.
48. Sumita, M.; Sakata, K.; Asai, S.; Miyasaka, K.; Nakagawa, H. *Polym. Bull.* **1991,** *25*, 265.
49. Dharaiya, D.; Jana, S. C. *Polymer* **2005,** *46*, 10139.
50. Averous, L. http://www.biodeg.net/bioplastic.html, **2011.**